Quantitative in-situ TEM nanotensile testing of single crystal Ni facilitated by a new sample preparation approach

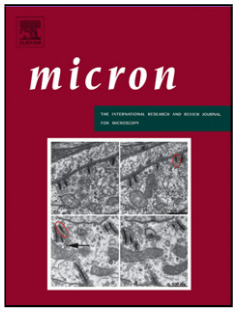

Title: Quantitative *in-situ* TEM nanotensile testing of single crystal Ni facilitated by a new sample preparation approach

Author: Vahid Samaeeaghmiyoni Hosni Idrissi Jonas Groten Ruth Schwaiger Dominique Schryvers

PII: S0968-4328(16)30329-8
DOI: http://dx.doi.org/doi:10.1016/j.micron.2016.12.005
Reference: JMIC 2377

To appear in: *Micron*

Received date: 8-11-2016
Revised date: 13-12-2016
Accepted date: 15-12-2016

Please cite this article as: Samaeeaghmiyoni, Vahid, Idrissi, Hosni, Groten, Jonas, Schwaiger, Ruth, Schryvers, Dominique, Quantitative in-situ TEM nanotensile testing of single crystal Ni facilitated by a new sample preparation approach.Micron http://dx.doi.org/10.1016/j.micron.2016.12.005

Title

Quantitative *in-situ* TEM nanotensile testing of single crystal Ni facilitated by a new sample preparation approach

---

Vahid Samaeeaghmiyoni[a,*], Hosni Idrissi[a,c,§], Jonas Groten[b,§§], Ruth Schwaiger[b], Dominique Schryvers[a]

[a] Electron Microscopy for Materials Science (EMAT), Department of Physics, University of Antwerp, Groenenborgerlaan 171, B-2020 Antwerp, Belgium

[b] Institute for Applied Materials, Karlsruhe Institute of Technology (KIT), Hermann-von-Helmholtz-Platz 1, 76344 Eggenstein-Leopoldshafen, Germany

[c] Institute of Mechanics, Materials and Civil Engineering, Université catholique de Louvain, Place Sainte Barbe 2, B-1348 Louvain-la-Neuve, Belgium

§ now at: Institute of Mechanics, Materials and Civil Engineering, Université catholique de Louvain, Place Sainte Barbe 2, B-1348 Louvain-la-Neuve, Belgium

§§ now at: Joanneum Research, Leonhardstraße 59, 8010 Graz; Austria

* Corresponding author

vahid.Samaeeaghmiyoni@uantwerpen.be

hosni.idrissi@uantwerpen.be

jonas.groten@gmx.de

ruth.schwaiger@kit.edu

nick.schryvers@uantwerpen.be

Highlights

- A new sample preparation method for quantitative in-situ TEM tensile testing,
- Combination of twin jet electro polishing and focused ion beam,
- Possible to prepare the samples with pre-defined orientation and with specific defects,
- Resulted less FIB-affected samples proper for plasticity investigation,
- The FIB induced defects at edges act as dislocation sources.

Abstract

Twin-jet electro-polishing and Focused Ion Beam (FIB) were combined to produce small size Nickel single crystal specimens for quantitative *in-situ* nanotensile experiments in the transmission electron microscope. The combination of these techniques allows producing samples with nearly defect-free zones in the centre in contrast to conventional FIB-prepared samples. Since TEM investigations can be performed on the electro-polished samples prior to *in-situ* TEM straining, specimens with desired crystallographic orientation and initial microstructure can be prepared. The present results reveal a dislocation nucleation-controlled plasticity, in which small loops induced by FIB near the edges of the samples play a central role.

Keywords

Twin-jet electro-polishing, Focused Ion Beam, *In-situ* TEM tensile test, FIB-induced damages, Size effect.

1. Introduction

Recently, small-scale structures and materials are attracting a lot of attention of the materials science community due to high demands for smaller, more flexible and reliable microelectronics and micromechanical components, for example, in Micro-Electro-Mechanical Systems (MEMS) (Gravier et al., 2009; Spearing, 2000). Aside from the challenges of the synthesis of such size-reduced materials, the investigation of their mechanical properties and deformation mechanisms raises several new challenges.

Recent advances in different electron microscopy (EM) techniques and of MEMS components now enable the simultaneous investigation of structural and mechanical properties using *in-situ* EM mechanical tests. Materials with reduced dimensions can be deformed using tensile deformation, compression, nanoindentation, and bending in either a scanning electron microscope (SEM) (Kiener et al., 2009; Kiener et al., 2006; Moser et al., 2005; Schwaiger et al., 2012; Uchic et al., 2004), or a

transmission electron microscope (TEM) (De Knoop and Legros, 2014; Idrissi et al., 2016; Imrich et al., 2015; Kiener et al., 2012a; Kiener and Minor, 2011b; Kiener et al., 2012b; Louchet and Saka, 2003; Minor et al., 2001; Oh et al., 2009; Shan et al., 2008).

The sample dimensions play an important role in the mechanical behaviour and active deformation mechanisms. Usually the attained material strength inversely scales with sample dimensions, i.e., thin film thickness or pillar and wire diameter (Greer and De Hosson, 2011; Zhu et al., 2008). For example, the inverse scale-strength behaviour of small-sized single crystalline materials is mainly attributed to the lack of dislocation sources in the sample (Lee et al., 2009), dislocation source exhaustion due to the presence of truncated spiral dislocation sources (Kiener et al., 2012a), and enhanced dislocation starvation at the surface (Shan et al., 2008).

However, in the case of TEM research, most samples need to be trimmed and/or thinned and so in order to properly interpret the experimental data, artefacts induced by these thinning procedures need to be avoided or at least well documented. The sample preparation method used in most *in-situ* SEM and TEM mechanical tests is Focused Ion Beam (FIB) thinning. Site selectivity, the range of materials for which FIB can be used, micro-level manipulation ability, machining flexibility as well as speed and reliability make FIB a very versatile technique for miniaturized sample preparation, in particular for TEM investigations (Mayer et al., 2007; Volkert and Minor). However, a thin amorphous layer at the surface (Kiener et al., 2007; Marien et al., 1999), implanted ions (Kiener et al., 2007), induced defects, such as vacancies, self-interstitial atoms, stacking faults or dislocation loops (Jenkins and Kirk, 2001; Langford and Rogers, 2008), or even precipitations (Ghoniem et al., 2000; Kiritani et al., 1994; Victoria et al., 2000) as well as changes of the crystallographic orientation (Mayer et al., 2007) are major artefacts introduced by FIB (Idrissi et al., 2011). It has also been shown that such FIB damages can substantially affect the mechanical properties and the deformation mechanisms (Bei et al., 2007; Idrissi et al., 2011; Lee, 2011; Schneider et al., 2013; Shan et al., 2008; Shim et al., 2009) similar to other irradiation processes (Hosemann et al., 2008; Raghavan et al., 2010). For example, the amorphous layer can hinder the escape of the dislocations to the surface (Shan et al., 2008), implanted Ga may cause solid-solution hardening (Kiener et al., 2007), point defects and dislocation loops can pin glissile dislocations (Idrissi et al., 2011; Jenkins and Kirk, 2001) and facilitate nucleation of dislocations (Kiener et al., 2007; Lee, 2011; Marien et al., 1999; Schneider et al., 2013). Therefore, in most cases, the mechanical properties and the deformation mechanisms observed in conventional FIB-prepared samples in the micron and submicron range are not directly expandable to bulk materials. In order to avoid FIB for *in-situ* SEM/TEM mechanical testing, other techniques based on electro-chemical processing have been used to produce small-sized metallic systems (Bei et al., 2007; Shim et al., 2009; Zhang et al., 2009). However, these techniques are not site selective and cannot be used to produce well-defined specimens with respect to orientation, defect content, etc.

In the present work, a combination of twin-jet electro-polishing followed by FIB cutting has been used to minimize FIB damages on small-sized Ni specimens dedicated for *in-situ* TEM nanotensile testing experiments. Conventional twin-jet electro-polishing was used for thinning a Ni bulk sample, while FIB was only used for cutting and mounting the tensile sample on the dedicated MEMS device, i.e., not for (further) thinning (see also next section). This combination was used before in order to perform *in-situ* TEM environmental investigations (Zhong et al., 2016), in order to investigate the stress induced transformation in a shape memory alloy by a qualitative *in-situ* tensile test method

(Mao et al., 2013) and in order to decrease the FIB milling time to prepare micropillars (Moser et al., 2012). In the latter case, twin-jet electro-polishing was used to remove most of the material, and FIB was used for final micro-machining and shaping of the samples. Also in most cases, final thinning was performed with FIB, which is avoided in the present work. The aim of the present study is to design a method with which a nanotensile micron-sized sample can be produced for a quantitative *in-situ* TEM tensile experiment with a central area (nearly) free of artefacts in which the pristine response to the applied stress can be investigated.

It is also worth noting that, because TEM thin foils prepared by twin-jet electro-polishing can be investigated prior to *in-situ* TEM straining, specimens with a pre-defined, selected crystallographic orientation and well-characterized initial microstructure can be obtained. This facilitates, for example, studying specific grain boundaries or defined initial dislocation densities in high resolved shear stress situations and two-beam conditions for proper diffraction contrast imaging. In the literature, similar efforts have been made by combining electron backscatter diffraction (EBSD) and FIB for the preparation of *in-situ* TEM samples with specific grain, twin or phase boundaries (Kiener and Minor, 2011a, 2011b). However, other crucial information such as the initial dislocation density and structure, the local structure of the interfaces as well as the orientation of these interfaces below the surface, cannot be extracted from EBSD. Furthermore, as in these cases final FIB thinning cannot be avoided, the analyses of the genuine deformation mechanisms during *in-situ* TEM straining remain very difficult, if not impossible.

2. Materials and methods

Discs of 3 mm diameter and a thickness of ~100 µm were prepared from a high purity Ni foil (99.999%) (Goodfellow GmbH, Bad Nauheim, Germany). The discs were annealed for 1 hour at 400°C under high vacuum conditions in order to relax internal stresses in the structure. An average grain size of 18 µm after the heat treatment was calculated from EBSD mapping. The discs were then twin-jet electro-polished with a solution of Perchloric acid and Acetic acid, 1:4, in a Tenupol 3 instrument (Struers ApS, Ballerup, Denmark) at 0°C, 18-19 V, 100 mA and immediately rinsed with Methanol and distilled water.

In order to select the appropriate position and crystallographic orientation for the tensile test samples, conventional TEM techniques including selected area diffraction (SAD) and bright field TEM (BF-TEM) were used on the electro-polished samples in an Osiris TEM (FEI Company, Hillsboro, OR USA) operating at 200 kV. The following key parameters were taken into account: i) The sample location was selected from electron transparent regions, which is needed for the *in-situ* TEM experiment (Fig. 1a). ii) The length of the sample (i.e., tensile direction) was selected parallel to the edge of the hole from the electro-polishing process, in order to obtain a uniform cross-section over the gage length (Fig. S1 of the supplementary material). This ensures a homogenous applied stress during the *in-situ* tests (Fig. 1b). iii) The tensile sample was selected from a dislocation-free grain (after checking the grain in various two-beam conditions, Fig. S2 of the supplementary material).

The *in-situ* nanotensile tests were performed in compression mode using a conductive diamond flat punch indenter in the PI 95 TEM PicoIndenter instrument (Hysitron, Inc., Minneapolis, MN, USA). A special MEMS device, referred to as *push-to-pull* (PTP) device, was used to transform the compression into a tensile mode. Owing to four identical springs distributed symmetrically at the

corners of this device (Fig. 1c), the compression loading (push) of the flat punch indenter on the semi-circular end of the PTP device is converted into a uniaxial tension loading (pull) on the middle gap of the PTP device (Fig. 1c). The springs are arranged in such a way that the force acting on them is parallel to the force on the tensile specimen. The transducer of the PI 95 TEM PicoIndenter offers both displacement-control and load-control indentation modes, and exhibits load and displacement resolutions below 3 nN and 0.02 nm, respectively. The load and displacement noise floors are approximately 200 nN and 0.4 nm, respectively.

In the present study, the spring constant of the PTP device was equal to 150 N/m. In order to perform the *in-situ* TEM tensile tests the displacement-control mode was used. The raw force data obtained from the indenter holder is a combination of the force applied on the tensile sample and that on the PTP device springs. The force on the Ni sample was extracted by subtracting the contribution of the PTP device from the raw force. The engineering stress was obtained by dividing the force on the sample by the cross-sectional area measured on SEM images after fracture of the sample but from a location away from the fracture site (see also Fig. S4 of the supplementary material), while the engineering strain was calculated by dividing the raw displacement data by the initial gage length measured on the plan-view SEM images (Fig. 1d). The raw displacement data was measured frame-by-frame on the recorded TEM videos using digital image correlation.

To cut, lift and mount the sample on the PTP device, a Helios Nanolab 650 dual beam FIB/SEM (FEI Company, Hillsboro, OR, USA) was used. At first, a sample of roughly 8 µm length and 2-3 µm width was cut from the electro-polished foil using an ion beam of 30kV / 80pA and transferred to the PTP device using a micromanipulator (Oxford Instruments plc, Tubney Woods, UK) (Fig. 1b). The sample was then attached to the PTP device by electron beam deposited platinum (Fig. 1d). In order to avoid Ga^+ ion beam damage to the gage section as much as possible during the transfer of the tensile sample to the PTP device, the tensile sample was only locally exposed to the ion beam, outside the gage section used for the tensile test. Then, the width of the tensile sample in the middle gap of the PTP was reduced to around 1 µm using an ion beam of 30kV/80pA (Fig. 1d). The main difference with other combined techniques is that in the present case the ion beam is used neither for further thinning nor for imaging of the sample. In other words, the Ga^+ ion beam is oriented perpendicular to the surface and only touches the sample for cutting its edges. Diffraction contrast imagining, high resolution TEM (HRTEM), and scanning transmission electron microscope (STEM) together with energy dispersive X-ray spectroscopy (EDX) mapping have been used to characterize the microstructural and chemical changes induced by the FIB cuts at the edges of the tensile sample as well as the effects of the tensile deformation.

3. Results and discussion

Fig. 2a shows a BF-TEM image of the tensile sample mounted on the PTP device before deformation. The sample dimensions are $3074 \pm 7\ \mathrm{nm} \times 990 \pm 7\ \mathrm{nm} \times 54 \pm 3\ \mathrm{nm}$. This sample was oriented for multiple slip with the tensile axis parallel to the $[\bar{1}\ 1\ \bar{1}]$ direction, and the pole normal to the foil surface was close to $[\bar{2}\ 1\ 3]$. In this case, a maximum Schmid factor (m) of 0.27 can be reached in the$(1\ 1\ 1)[\bar{1}\ 1\ 0]$, $(1\ 1\ 1)[0\ \bar{1}\ 1]$, $(\bar{1}\ \bar{1}\ 1)[1\ 0\ 1]$, $(\bar{1}\ \bar{1}\ 1)[\bar{1}\ 1\ 0]$, $(1\ \bar{1}\ \bar{1})[1\ 1\ 0]$ and $(1\ \bar{1}\ \bar{1})[0\ \bar{1}\ 1]$ slip systems, while m is equal to 0 for the other 6 systems.

As can be seen in Fig. 2a the reduction of the sample width by the FIB cut has severely affected the edges, while the centre of the sample, indicated with a dashed ellipse, is nearly damage-free; there are still a few discrete small FIB damage sites, seen as black dots in the centre, resulting from the fact that the ion beam used for cutting out the sample from the electro-polished foil and trimming the edges will always have a certain spread with some Ga ions straying further away from the edge towards the centre of the sample and creating some dislocation loops in the nearly-damage free area. Along the edges two types of FIB induced defect areas (labelled A and B) can be observed. Area A, enlarged in Fig. 2b, exhibits a ripple shaped contrast similar to that observed in FIB irradiated Cu and Fe-Cr alloy (Jin et al., 2010; Kiener et al., 2007) and is expected to be due to the strong diffraction contrast of the dislocation structure formed from the superposition and interaction of dislocation loops and the formation of long parallel tangled dislocation structures. From Fig. 2c, the defects in area B can be identified as small dislocation loops with a diameter up to 50 nm, and it can be seen that the size of the loops increases towards the edge of the sample. However, smaller loops remain the majority. Dislocation loops generated by the collapse of vacancies or interstitials are indeed frequently observed in irradiated materials (Yao et al., 2008).

The HRTEM image of Fig. 3a reveals details of the defects from area A in Fig. 2a. In this figure, the strong strain field associated with long dislocations can still be observed. The HRTEM of Fig. 3b was obtained in area B of Fig. 2a. It shows that the FIB-induced dislocation loops are planar defects lying in the $\{1\ 1\ 1\}$ planes. Such feature is typical of interstitial or vacancy type stacking faults delimited by Frank partial dislocations with Burgers vector $\frac{a}{6}[1\ 1\ 2]$ (Idrissi et al., 2011). In the present study, the small size of these defects (compared to the thickness of the tensile sample) as well as the strong strain field surrounding them makes their individual identification at the atomic scale extremely difficult and is beyond the scope of this paper.

The chemical composition of areas near the edges of the tensile sample was investigated using STEM-EDX mapping. Fig. 4a shows a High Angle Annular Dark Field (HAADF)-STEM image, in which FIB damages at the edge are still visible due to the high strain field and moderate camera length. 10±1 at.% Ga was measured in the area delimited by the white rectangle in Fig. 4a. Fig. 4b shows a Ga rich strip of ~50 nm at the edge of the sample. In that region the Ga atoms are distributed in a uniform manner and neither precipitate nor segregate at the defects (see also Fig. S3 of the supplementary material). Still, some weaker Ga traces are recognized further away from the edge, as seen in Fig. 4d, which is due to a slight spreading of the Ga ion beam.

These results indicate that by using this combined procedure of electro-polishing thinning and FIB cutting, genuine deformation defects and plasticity mechanisms can be investigated in the almost FIB damage-free area in the centre of the sample. For example, the intrinsic mobility of deformation dislocations can be measured in the absence of severe FIB damage, which could act as obstacles for moving dislocations. The characterization of the mechanisms controlling the interaction of deformation dislocations with pre-selected structural boundaries can be achieved in samples with interfaces located in the centre of the sample. Indeed, such interactions can be highly affected by the FIB-induced defects in the vicinity or inside the boundaries in cross-sectional samples prepared only by FIB. The method can also be used to observe strengthening mechanisms in samples containing nano-precipitates or dispersed small particles. Indeed, the discrimination between these

defects and the FIB-induced loops or precipitates can be expected to be extremely difficult (at least at the low magnification scale required to observe the interaction between the defects and moving dislocations during *in-situ* TEM straining). Moreover, as will be shown below, the remaining FIB-induced defects at the edges of the sample can be used to the advantage of the experiment.

Fig. 5a shows a BF-TEM snapshot obtained during the *in-situ* tensile deformation of the sample shown in Fig. 1 at $\varepsilon = 0.018$ and $\sigma = 2743$ MPa. The experiment was carried out at an initial strain rate of $3.3e^{-4}s^{-1}$. In this figure, three slip traces caused by the glide of dislocations in the $(\bar{1}\ 1\ 1)$, $(\bar{1}\ \bar{1}\ 1)$ and $(1\ 1\ 1)$ glide planes can be seen as in the $(\bar{2}\ 1\ 3)$ stereographic projection of Fig. 5b. These dislocations nucleated from the edge of the sample damaged by the FIB cut. In Fig. 5c, dislocations nucleated from the left edge in the $(\bar{1}\ 1\ 1)$ plane and stopping close to the right edge of the tensile sample can be observed after unloading. Note the 'clean' diffraction contrast of these dislocations due to the absence of severe FIB damage in the centre of the sample. Although the three observed slip planes exhibit identical Schmid factors (0.27), it can be concluded from Fig. 5a that the slip traces ST3 and ST2 induced by the glide of dislocations in the $(\bar{1}\ 1\ 1)$ and $(\bar{1}\ \bar{1}\ 1)$ planes, respectively, are dominant. This can be attributed to the nature of the dislocation sources on the edge of the sample and induced by FIB and/or to inaccuracies in the mounting procedure of the sample on the PTP device which can induce small deviations between the gage length axis and the tensile axis leading to changes in the resolved shear stresses on dislocations. Still, these results confirm that the FIB damage induced at the edges can act as preferential sites for the nucleation of dislocations while the nearly damage-free centre of the sample is well-suited for the determination of the dislocations and their response to the *in-situ* deformation. Also, the participation of the FIB defects as dislocation sources prevents early fracture due to the lack of dislocation sources in such small samples (Kiener et al., 2012a; Lu et al., 2011).

Fig. 6 shows the engineering stress - engineering strain curve extracted from the above *in-situ* TEM tensile test. Young's modulus extracted from the loading part of Fig. 6 equals 220 GPa, very close to Young's modulus of bulk polycrystalline pure Ni (207 GPa (Davis, 2000)). However, the calculated Young's modulus using the elastic constants for the [1 1 1] orientation is 303 GPa (Ledbetter and Reed, 1973), while the average modulus determined for micropillars of the same orientation was 308 GPa with a standard deviation of 79 GPa (Frick et al., 2008). The smaller value observed in our case can be due to either a slight misalignment of the sample and the tensile direction resulting in a lower modulus (since the modulus along the [1 1 1] direction is the maximum one) or to a size effect related to the effect of the surface elastic modulus on thin samples (Ronald and Vijay, 2000). Furthermore, a high yield stress of 2.5 GPa can be measured from the graph of Fig. 6 in agreement with values of ~3 GPa reported in a single-crystalline Ni nanopillar with a diameter of 165 nm (Frick et al., 2008). The small difference in slope between the loading and unloading parts is expected to be due to the existence of the plastic regime and the bending of the nanoscale sample without breaking during unloading.

The plastic behaviour of such small-sized specimens is often controlled by the dislocation nucleation stage. For a dislocation source, such as a Frank-Read (F-R) source or a loop, a critical resolved shear stress is needed to expel a dislocation from the F-R source or to expand the loop. The critical resolved shear stress, τ, for a dislocation to form is controlled by the line tension and can be approximated by equation (1) (Hull and Bacon, 2011):

$$\tau = \frac{\mu b}{2r} \qquad (1)$$

where μ is the shear modulus of the material (76 GPa for the bulk single crystal value) (Schneider et al., 2013)), *b* is the magnitude of the Burgers vector of a perfect glissile dislocation of type $\frac{a}{2}[110]$ (0.24 nm), and *r* is the source radius. The 2.5 GPa engineering yield stress (σ) measured in the sample of Fig. 6 corresponds to a critical resolved shear stress of 680 MPa taking into account the corresponding Schmid factor (m) of 0.27 via Schmid's law, equation 2:

$$\tau = \sigma \cdot m \qquad (2)$$

This corresponds to the critical resolved shear stress of a dislocation source with a radius of ~ 15 nm which is consistent with the size of the FIB-induced loops observed at the edge of the sample (Fig. 2). Furthermore, in such a thin sample the image forces are relatively large so they can accelerate the escape of the dislocations to the free surfaces. However, the critical stress for source opening might not be the only limiting factor. Indeed, because the FIB-induced loops are sessile Frank faulted loops (Idrissi et al., 2011), the critical stress for operating the source will also be controlled by the transformation of Frank faulted loops into perfect loops. Molecular dynamic simulations (Kadoyoshi et al., 2007) have revealed that unfaulting of Frank loops could occur under an external shear stress by the creation and the sweep across the loop of Shockley partial dislocations following the reactions

$\frac{1}{3}\langle 1\,1\,1\rangle + \frac{1}{6}\langle 1\,1\,\bar{2}\rangle \rightarrow \frac{1}{2}\langle 1\,1\,0\rangle$ reaction (1)

$\frac{1}{3}\langle 1\,1\,1\rangle + \frac{1}{6}\langle \bar{1}\,2\,\bar{1}\rangle \rightarrow \frac{1}{6}\langle 1\,4\,1\rangle$ reaction (2)

$\frac{1}{6}\langle 1\,4\,1\rangle + \frac{1}{6}\langle 2\,\bar{1}\,\bar{1}\rangle \rightarrow \frac{1}{2}\langle 1\,1\,0\rangle$ reaction (3)

For a vacancy Frank loop, reaction (1), and for an interstitial Frank loop, reactions (2) and (3), are required. Because such reactions are energetically unfavorable, high stress levels (such as those attained in the present study) are required. Furthermore, on the basis of elasticity theory, the energy of the perfect loop becomes significantly smaller than that of the Frank faulted loop if the loop size exceeds some critical radius (Kroupa, 1966). In face-centered cubic (FCC) metals with high stacking fault energy, such as Ni and Al, this critical limit is very small (in Al, the perfect loop is energetically favorable for any size (Hull and Bacon, 2011)). Therefore, large Frank loops can transform into unfaulted loops even without the presence of external stress.

To sum up this part, larger dislocation loops in the investigated Ni sample, regardless of their types, faulted or unfaulted, can open and participate in deformation at lower stress levels. Most of the large dislocation loops in the Ni sample, having high stacking fault energy, are likely unfaulted according to the small critical size for stability of faulted loops and larger loops need lower shear stress for opening following eq. 1. For faulted dislocation loops, simulations have also proven that their unfaulting stress decreases as the size of the dislocation loop increases (Kadoyoshi et al., 2007).

From Fig. 6 a very high strain hardening rate of 43 GPa is measured in the macroscopic plastic regime. Similar behaviour has been reported for Ni single crystal nanopillars with a diameter of ~156 nm and compressed along the $< 1\,1\,1 >$ direction (Frick et al., 2008). Observed size effects on the strain hardening of micron and sub-micron samples are generally attributed to either the formation and development of dislocation structures (Kiener et al., 2011) or to dislocation source exhaustion

and dislocation starvation (Kiener and Minor, 2011a; Shan et al., 2008). However, in the present case, none of these cases was observed. The high strain hardening can, thus, be attributed to the nucleation of dislocations from the different sized dislocation loops. The plastic deformation starts when the stress level is high enough to activate large loops. To accommodate further plastic deformation, more dislocation loops that are smaller will be activated, which requires an increase of the applied stress leading to strain hardening.

From the video provided in the supplementary material, it can further be noticed that the load drops (indicated by the black arrows in Fig. 6) were accompanied by simultaneous nucleation and glide of high numbers of dislocations from the defect areas at the edges of the specimen. Interestingly, the magnitude of the load drops increased with increasing strain indicating that the number of dislocations participating in the deformation process increased with the plastic strain, which is in agreement with our observations of a greater number of smaller than larger loops being present, the latter being the first to act as dislocation sources.

The present work provides a new approach to quantitative *in-situ* TEM tensile testing of micron-sized samples. The dedicated sample preparation method not only yields a nearly defect-free central area, in which pristine dislocation movement can be followed, but the FIB artefacts are even beneficial and can be used to the advantage of the experiment as they provide the dislocation sources needed to avoid premature fracture. The present approach can also be used for *in-situ* TEM tensile testing of samples containing a single defect, such as a grain or twin boundary in the centre of the sample, since such a defect can be identified and characterized by conventional TEM on the electro-polished sample before the final FIB cutting is performed.

4. Conclusions

In the present work, a combination of twin-jet electro-polishing for thinning to TEM transparency and FIB cutting for final shape selection has been used to prepare micron-sized Ni specimens with pre-selected orientation for *in-situ* TEM nanotensile experiments. The centre of the sample is nearly free of FIB induced artefacts, while a Ga-rich layer, long dislocations and dislocation loops have been induced at the edges of the sample due to the FIB cut. The latter artefacts at the sample edges were found to act as nucleation sites for deformation dislocations during the *in-situ* TEM straining, which prevents early fracture typically caused by the lack of sufficient dislocation sources in micron-sized samples. Strain hardening was observed and attributed to an increase of the stress level required for the opening of dislocation loops with different radius with increasing deformation. These results constitute the first step towards a better control of sample preparation techniques for quantitative *in-situ* TEM nanomechanical testing of materials.

Acknowledgments

This research has been performed with the financial support of the Belgian Science Policy (Belspo) under the framework of the interuniversity attraction poles program, IAP7/21. Financial support from the Flemish (FWO) and German Research Foundation (DFG) through the European M-ERA.NET project “FaSS“ (Fatigue Simulation near Surfaces) under the grant numbers GA.014.13N and SCHW855/5-1, respectively, is gratefully acknowledged. V. Samaeeaghmiyoni also acknowledges the FWO research project G012012N “Understanding nanocrystalline mechanical behaviour from

structural investigations". H. Idrissi is currently mandated by the Belgian National Fund for Scientific Research (FSR-FNRS).

References

Bei, H., Shim, S., George, E.P., Miller, M.K., Herbert, E.G., Pharr, G.M., 2007. Compressive strengths of molybdenum alloy micro-pillars prepared using a new technique. Scripta Materialia 57, 397-400.
Davis, J.R., 2000. ASM Specialty Handbook: Nickel, Cobalt, and Their Alloys. ASM International, The United States of America.
De Knoop, L., Legros, M., 2014. Absorption of crystal/amorphous interfacial dislocations during in situ TEM nanoindentation of an Al thin film on Si. Scripta Materialia 74, 44-47.
Frick, C.P., Clark, B.G., Orso, S., Schneider, A.S., Arzt, E., 2008. Size effect on strength and strain hardening of small-scale [1 1 1] nickel compression pillars. Materials Science and Engineering: A 489, 319-329.
Ghoniem, N.M., Singh, B.N., Sun, L.Z., Díaz de la Rubia, T., 2000. Interaction and accumulation of glissile defect clusters near dislocations. Journal of Nuclear Materials 276, 166-177.
Gravier, S., Coulombier, M., Safi, A., Andre, N., Boe, A., Raskin, J.P., Pardoen, T., 2009. New On-Chip Nanomechanical Testing Laboratory - Applications to Aluminum and Polysilicon Thin Films. Journal of Microelectromechanical Systems 18, 555-569.
Greer, J.R., De Hosson, J.T.M., 2011. Plasticity in small-sized metallic systems: Intrinsic versus extrinsic size effect. Progress in Materials Science 56, 654-724.
Hosemann, P., Swadener, J.G., Kiener, D., Was, G.S., Maloy, S.A., Li, N., 2008. An exploratory study to determine applicability of nano-hardness and micro-compression measurements for yield stress estimation. Journal of Nuclear Materials 375, 135-143.
Hull, D., Bacon, D.J., 2011. Introduction to Dislocations, Fifth ed. Butterworth-Heinemann, Oxford.
Idrissi, H., Bollinger, C., Boioli, F., Schryvers, D., Cordier, P., 2016. Low-temperature plasticity of olivine revisited with in situ TEM nanomechanical testing. Science Advances 2.
Idrissi, H., Turner, S., Mitsuhara, M., Wang, B., Hata, S., Coulombier, M., Raskin, J.-P., Pardoen, T., Tendeloo, G.V., Schryvers, D., 2011. Point Defect Clusters and Dislocations in FIB Irradiated Nanocrystalline Aluminum Films: An Electron Tomography and Aberration-Corrected High-Resolution ADF-STEM Study. Microscopy and Microanalysis 17, 983-990.
Imrich, P.J., Kirchlechner, C., Kiener, D., Dehm, G., 2015. Internal and external stresses: In situ TEM compression of Cu bicrystals containing a twin boundary. Scripta Materialia 100, 94-97.
Jenkins, M.L., Kirk, M.A., 2001. Characterization of Radiation Damage by Transmission Electron Microscopy. IOP Publishing Ltd.
Jin, H.-h., Shin, C., Kwon, J., 2010. Fabrication of a TEM sample of ion-irradiated material using focused ion beam microprocessing and low-energy Ar ion milling Jornal of Electron Microscopy 59, 463-468.
Kadoyoshi, T., Kaburaki, H., Shimizu, F., Kimizuka, H., Jitsukawa, S., Li, J., 2007. Molecular dynamics study on the formation of stacking fault tetrahedra and unfaulting of Frank loops in fcc metals. Acta Materialia 55, 3073-3080.
Kiener, D., Guruprasad, P.J., Keralavarma, S.M., Dehm, G., Benzerga, A.A., 2011. Work hardening in micropillar compression: In situ experiments and modeling. Acta Materialia 59, 3825-3840.
Kiener, D., Kaufmann, P., Minor, A.M., 2012a. Strength, Hardening, and Failure Observed by In Situ TEM Tensile Testing. Advanced Engineering Materials 14, 960-967.
Kiener, D., Minor, A.M., 2011a. Source-controlled yield and hardening of Cu(1;0;0) studied by in situ transmission electron microscopy. Acta Materialia 59, 1328-1337.
Kiener, D., Minor, A.M., 2011b. Source Truncation and Exhaustion: Insights from Quantitative in situ TEM Tensile Testing. Nano Letters 11, 3816-3820.
Kiener, D., Motz, C., Dehm, G., Pippan, R., 2009. Overview on established and novel FIB based miniaturized mechanical testing using in-situ SEM. International Journal of Materials Research 100, 1074-1087.

Kiener, D., Motz, C., Rester, M., Jenko, M., Dehm, G., 2007. FIB damage of Cu and possible consequences for miniaturized mechanical tests. Materials Science and Engineering: A 459, 262-272.
Kiener, D., Motz, C., Schöberl, T., Jenko, M., Dehm, G., 2006. Determination of Mechanical Properties of Copper at the Micron Scale. Advanced Engineering Materials 8, 1119-1125.
Kiener, D., Zhang, Z., Šturm, S., Cazottes, S., Imrich, P.J., Kirchlechner, C., Dehm, G., 2012b. Advanced nanomechanics in the TEM: effects of thermal annealing on FIB prepared Cu samples. Philosophical Magazine 92, 3269-3289.
Kiritani, M., Fukuta, Y., Mima, T., Iiyoshi, E., Kizuka, Y., Kojima, S., Matsunami, N., 1994. Formation of vacancy clustered defects from cascade collisions during heavy-ion irradiation and their annihilation by freely-migrating interstitial atoms. Journal of Nuclear Materials 212–215, Part 1, 192-197.
Kroupa, F., 1966. Dislocation Dipoles and Dislocation Loops. Journal de Physique Colloques 27 (C3), 154-167.
Langford, R.M., Rogers, M., 2008. In situ lift-out: Steps to improve yield and a comparison with other FIB TEM sample preparation techniques. Micron 39, 1325-1330.
Ledbetter, H.M., Reed, R.P., 1973. Elastic Properties of Metals and Alloys, I. Iron, Nickel, and Iron‐Nickel Alloys. Journal of Physical and Chemical Reference Data 2, 531-618.
Lee, S.-W., Han, S.M., Nix, W.D., 2009. Uniaxial compression of fcc Au nanopillars on an MgO substrate: The effects of prestraining and annealing. Acta Materialia 57, 4404-4415.
Lee, S.W., 2011. The Plasticity of Metals at The Sub-Micronmeter Scale and Dislocation Dynamics in A Thin Film Materials Science and Engineering. Stanford University, p. 162.
Louchet, F., Saka, H., 2003. Comments on the paper: observation of dislocation dynamics in the electron microscope, by B.W. Lagow et al. Materials Science and Engineering: A 352, 71-75.
Lu, Y., Peng, C., Ganesan, Y., Yu Huang, J., 2011. Quantitative in situ TEM tensile testing of an individual nickel nanowire. Nanotechnology 22, 1-6.
Mao, S.C., Li, H.X., Liu, Y., Deng, Q.S., Wang, L.H., Zhang, Y.F., Zhang, Z., Han, X.D., 2013. Stress-induced martensitic transformation in nanometric NiTi shape memory alloy strips: An in situ TEM study of the thickness/size effect. Journal of Alloys and Compounds 579, 100-111.
Marien, j., Plitzko, J.M., Spolenak, R., Keller, R.-M., Mayer, J., 1999. Quantitative electron spectroscopic imaging studies of microelectronic metallization layers. Journal of Microscopy 194, 71-78.
Mayer, J., Giannuzzi, L.A., Kamino, T., Michael, J., 2007. TEM Sample Preparation and FIB-Induced Damage. MRS BULLETIN 32, 400-407.
Minor, A.M., Morris, J.W., Stach, E.A., 2001. Quantitative in situ nanoindentation in an electron microscope. Applied Physics Letters 79, 1625-1627.
Moser, B., Kuebler, J., Meinhard, H., Muster, W., Michler, J., 2005. Observation of Instabilities during Plastic Deformation by in-situ SEM Indentation Experiments. Advanced Engineering Materials 7, 388-392.
Moser, G., Felber, H., Rashkova, B., Imrich, P.J., krichlechner, C., Grosinger, W., Motz, C., Dehm, G., Kiener, D., 2012. Sample Preparation by Metallography and Focused Ion Beam for Nanomechanical Testing Practical Metallography 49, 343-355.
Oh, S.H., Legros, M., Kiener, D., Dehm, G., 2009. In situ observation of dislocation nucleation and escape in a submicrometre aluminium single crystal. Nature Materials 8, 95-100.
Raghavan, R., Boopathy, K., Ghisleni, R., Pouchon, M.A., Ramamurty, U., Michler, J., 2010. Ion irradiation enhances the mechanical performance of metallic glasses. Scripta Materialia 62, 462-465.
Ronald, E.M., Vijay, B.S., 2000. Size-dependent elastic properties of nanosized structural elements. Nanotechnology 11, 139.
Schneider, A.S., Kiener, D., Yakacki, C.M., Maier, H.J., Gruber, P.A., Tamura, N., Kunz, M., Minor, A.M., Frick, C.P., 2013. Influence of bulk pre-straining on the size effect in nickel compression pillars. Materials Science and Engineering: A 559, 147-158.

Schwaiger, R., Weber, M., Moser, B., Gumbsch, P., Kraft, O., 2012. Mechanical assessment of ultrafine-grained nickel by microcompression experiment and finite element simulation. Journal of Materials Research 27, 266-277.
Shan, Z.W., Mishra, R.K., Syed Asif, S.A., Warren, O.L., Minor, A.M., 2008. Mechanical annealing and source-limited deformation in submicrometre-diameter Ni crystals. Nat Mater 7, 115-119.
Shim, S., Bei, H., Miller, M.K., Pharr, G.M., George, E.P., 2009. Effects of focused ion beam milling on the compressive behavior of directionally solidified micropillars and the nanoindentation response of an electropolished surface. Acta Materialia 57, 503-510.
Spearing, S.M., 2000. Materials issues in microelectromechanical systems (MEMS). Acta Materialia 48, 179-196.
Uchic, M.D., Dimiduk, D.M., Florando, J.N., Nix, W.D., 2004. Sample Dimensions Influence Strength and Crystal Plasticity. Science 305, 986-989.
Victoria, M., Baluc, N., Bailat, C., Dai, Y., Luppo, M.I., Schäublin, R., Singh, B.N., 2000. The microstructure and associated tensile properties of irradiated fcc and bcc metals. Journal of Nuclear Materials 276, 114-122.
Volkert, C.A., Minor, A.M., Focused Ion Beam Microscopy and Micromachining. MRS BULLETIN 32, 389-399.
Yao, Z., Hernández-Mayoral, M., Jenkins, M.L., Kirk, M.A., 2008. Heavy-ion irradiations of Fe and Fe–Cr model alloys Part 1: Damage evolution in thin-foils at lower doses. Philosophical Magazine 88, 2851-2880.
Zhang, D., Breguet, J.M., Clavel, R., Phillippe, L., Utke, I., Michler, J., 2009. In situ tensile testing of individual Co nanowires inside a scanning electron microscope. Nanotechnology 20, 365706.
Zhong, X.L., Schilling, S., Zaluzec, N.J., Burke, M.G., 2016. Sample Preparation Methodologies for In Situ Liquid and Gaseous Cell Analytical Transmission Electron Microscopy of Electropolished Specimens. Microscopy and Microanalysis, 1-10.
Zhu, T.T., Bushby, A.J., Dunstan, D.J., 2008. Materials mechanical size effects: a review. Materials Technology 23, 193-209.

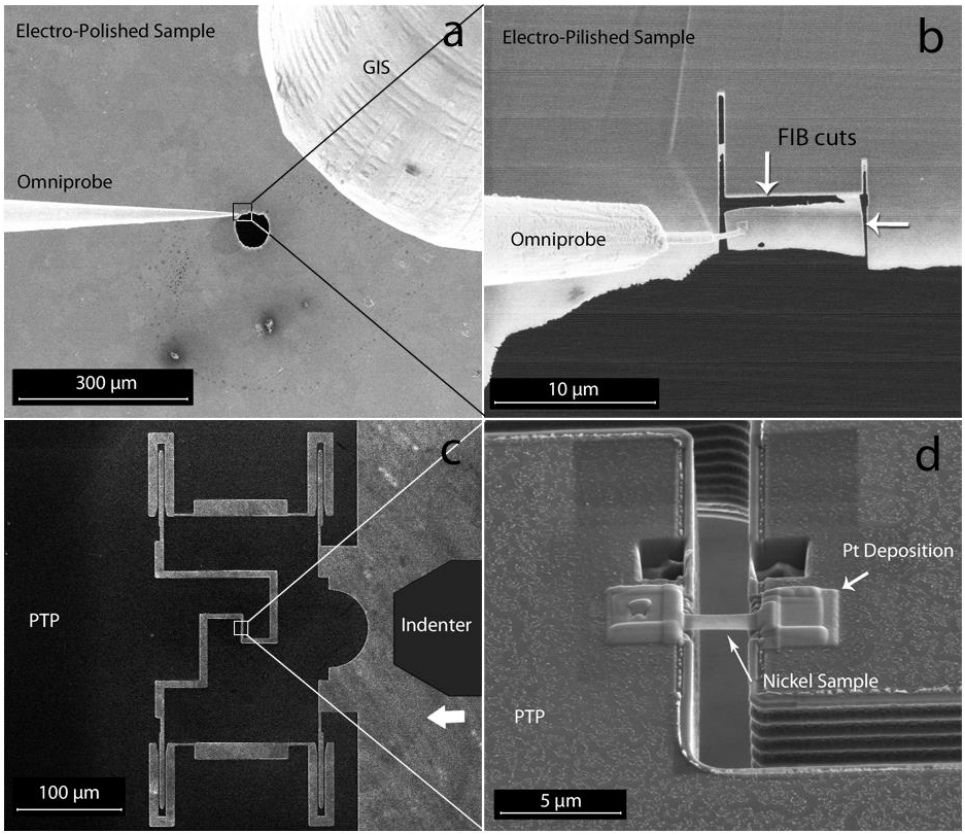

Fig. 1. SEM images showing the sequence of FIB preparation steps, (a) a low magnification view of the electro-polished foil with the Omniprobe micromanipulator and GIS needle for Pt deposition, (b) FIB cut from the thin electro-polished edge of the hole, (c) the PTP device, the schematic shape of indenter is manually added for clarity and the white arrow shows the force direction, and (d) mounting of the tensile sample on the PTP device using electron beam assisted deposited Pt.

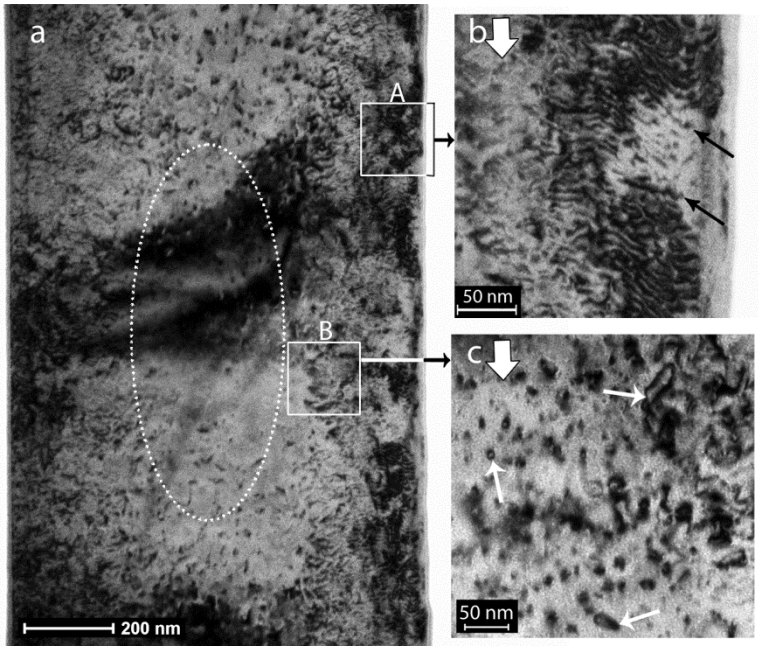

Fig. 2. (a) BF micrograph of sample before deformation, with highlighted regions A and B near the edges. (b) and (c) BF micrographs taken in two-beam condition with $\boldsymbol{g} = 1\,1\,\bar{1}$ (large white arrows) from area A containing tangled dislocation structure (black arrows) and area B containing different size dislocation loops (small white arrows), respectively.

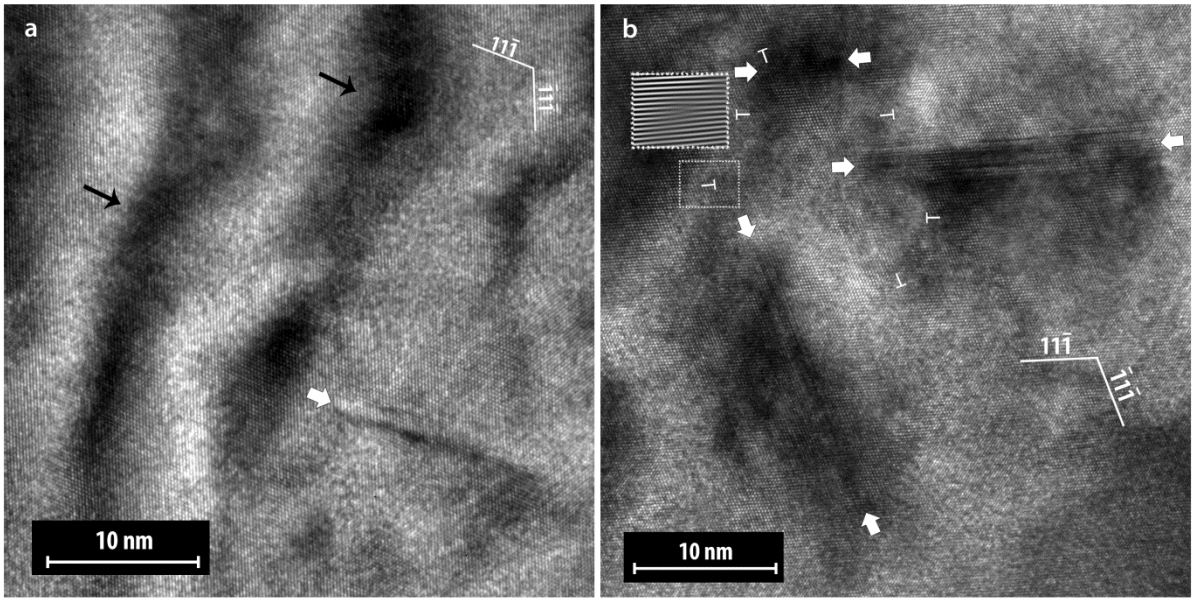

Fig. 3. HRTEM micrographs showing (a) FIB induced parallel dislocations indicated by black arrows from area A, and (b) nanoscale planar defects (white arrows) and some edge dislocations (⊥ mark) in area B.

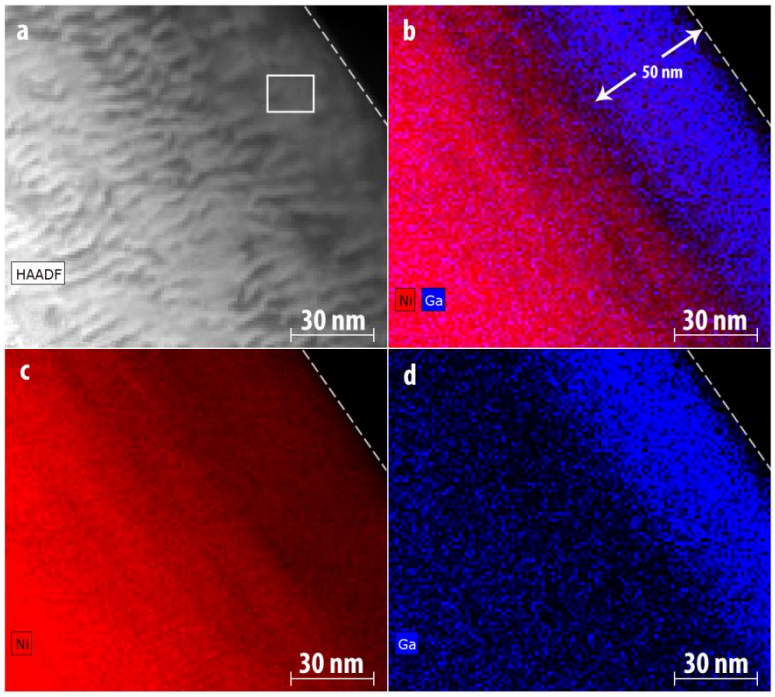

Fig. 4. (a) HAADF-STEM image, the Ga amount in the selected white rectangle is 10±1 at.% (using camera length of 330 mm still showing some dislocation contrast), (b) superposed HAADF-STEM image, Ni and Ga EDX chemical maps, (c) Ni EDX chemical map, and (d) Ga EDX chemical map.

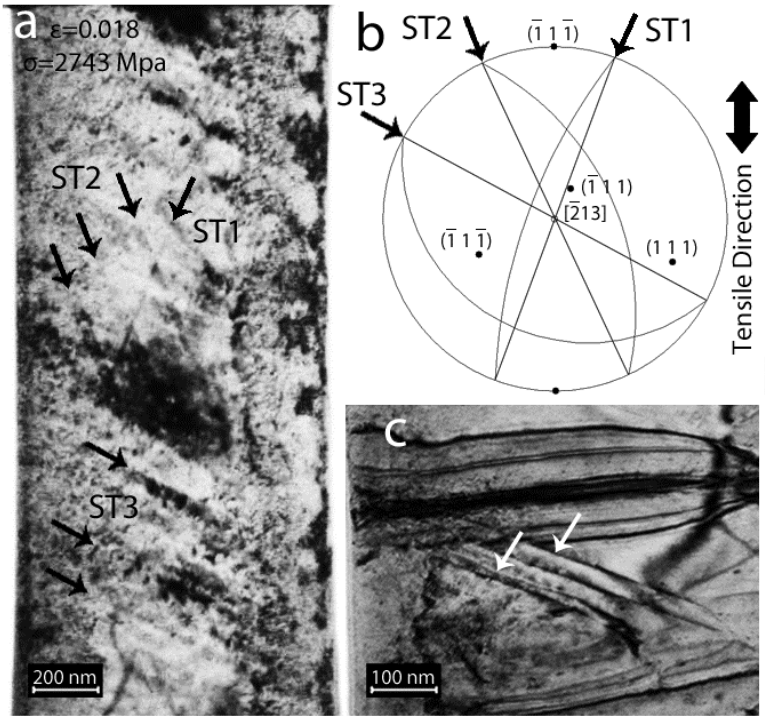

Fig. 5. (a) A BF-TEM snapshot taken during deformation at $\varepsilon = 0.018$ and $\sigma = 2743$ MPa. Three different slip traces (STs) can be observed, (b) the stereographic projection of the sample showing the intersections of {1 1 1} planes with the surface plane $(\bar{2}\,1\,3)$, and (c) the BF image of some deformation dislocations originating from the left edge and being halted after unloading.

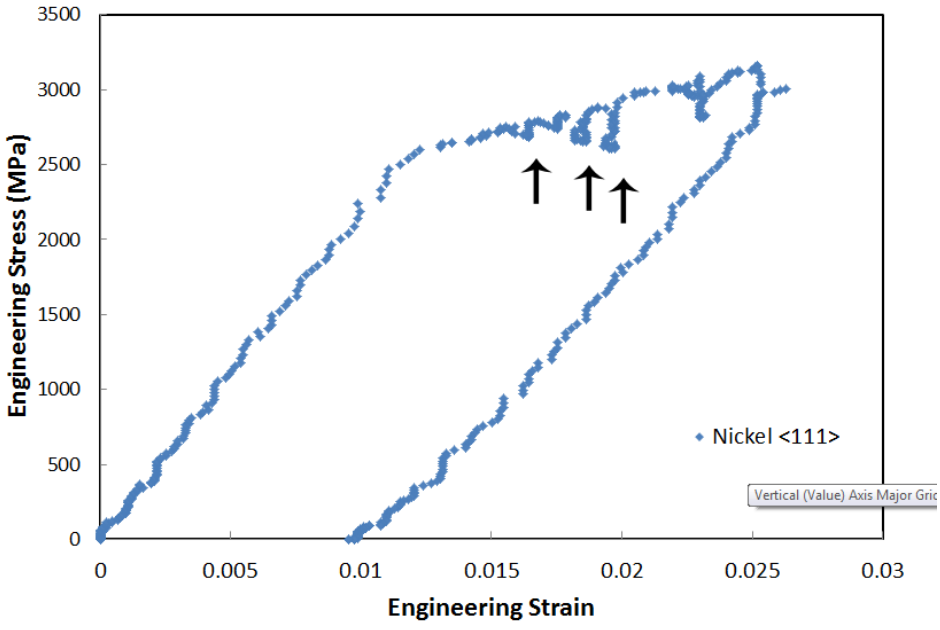

Fig. 6. The engineering stress - engineering strain curve extracted from the *in-situ* TEM nanotensile testing, the black arrows show increasing load drops with increasing deformation.